Sustainable Energy & Fuels

ROYAL SOCIETY OF CHEMISTRY

PAPER

View Article Online
View Journal | View Issue

Cite this: *Sustainable Energy Fuels*, 2022, **6**, 4716

Electrochemical ammonia synthesis *via* nitrate reduction on perovskite $La_xFeO_{3-\delta}$ with enhanced efficiency by oxygen vacancy engineering†

Qi Yin, Shihao Hu, Jingwen Liu and Hao Zhou *

Received 19th July 2022
Accepted 8th September 2022

DOI: 10.1039/d2se00997h

rsc.li/sustainable-energy

It is a novel and challenging task to seek an effective electrocatalyst to synthesize valuable ammonia from the harmful nitrate in the wastewater. This work innovatively applied the perovskite $La_xFeO_{3-\delta}$ ($x = 1$, 0.95, 0.9) as an electrocatalyst to reduce nitrate to ammonia. For the catalyst $L_{0.9}F$, the highest NH_3 yield was up to 1024.8 μg h^{-1} cm^{-2} at −1.0 V (*vs.* RHE), while the maximum faradaic efficiency was 78.1% achieved at −0.8 V (*vs.* RHE). The outstanding electrocatalytic activities were attributed to the oxygen vacancies generated from the A-site deficiencies. The N–O bonds were weakened with the oxygen atoms in the nitrate filling the oxygen vacancies. The adsorption and transformation of reaction intermediates were promoted due to the existence of oxygen vacancies. Meanwhile, the oxygen vacancies could serve as the active sites of the catalysts, and the deficiencies enhanced the charge transfer efficiency. This work provides a direction to fabricate efficient electrocatalysts for reducing nitrate to ammonia, which can effectively assist in handling both the energy crisis and the environmental pollution.

1. Introduction

Ammonia (NH_3) is a significant chemical raw material and hydrogen-rich fuel and plays an irreplaceable role in the chemical industry, agriculture, medicine and energy in modern society.[1,2] Currently, the Haber–Bosch process operated under high temperature (623–823 K) and high pressure (150–350 atm) is the dominant technology to synthesize ammonia in industry, despite its severe drawbacks such as high energy consumption, large carbon dioxide emission and the pressing need for high-purity H_2.[3,4] Therefore, it is urgent to find alternative ammonia synthesis technologies under mild conditions. The electrochemical nitrogen reduction reaction (NRR) is an ideal method to synthesize NH_3. However, the low efficiency of the NRR process owing to the high dissociation energy (941 kJ mol^{-1} for N≡N), low proton affinity and low solubility of N_2 hinders its industrialization.[1,3] Under such circumstances, electrochemical reduction of nitrate (NO_3^-) to ammonia has attracted the attention of scholars worldwide due to the relatively low dissociation energy of the N=O bond (204 kJ mol^{-1}).[1] Furthermore, nitrate is easily soluble and a significant pollutant in nature, making it a promising nitrogen source easier to utilize than the stable N_2 in air. Hence, large-scale ammonia production by the water-based electrochemical nitrate reduction reaction (NO_3RR) under ambient conditions is of dual significance both to alleviate the energy crisis and to reduce environmental pollution.

At present, the main challenges facing the large-scale ammonia production from the electrochemical NO_3RR are the high energy consumption and low ammonia selectivity caused by the high overpotential, multiple electron/proton transfer steps and competitive reactions.[1–3] Therefore, scholars worldwide are committed to searching for catalysts with high reaction activities and high ammonia selectivity. Recent studies have found that Cu and Cu-based materials have intense electrochemical NO_3RR activities for excellent intrinsic activity,[1–4] such as defect-rich metallic Cu nanoplates prepared through the *in situ* electroreduction of pre-synthesized CuO nanoplates,[1] Cu-incorporated crystalline 3,4,9,10-perylenetetracarboxylic dianhydride,[2] Cu/oxygen vacancy-rich Cu–Mn_3O_4,[3] metasequoia-like nanocrystals of CuFe prepared through doping Fe into Cu.[4] Illuminated by the Fe cofactor in nitrogenase in nature and the Fe active sites in Haber–Bosch catalysts,[4–6] Fe-based electrocatalysts have attracted great attention. Among them, the outstanding examples are Fe single-atom catalysts,[5] metal–organic framework-derived Co-doped Fe/Fe_2O_3,[6] and the metasequoia-like CuFe nanocrystals mentioned above.[4] Besides, transition metal elements such as Co[6–8] and Ni[9,10] have also been proved to have electrochemical NO_3RR activities. In general, the above non-noble-metal based electrocatalysts are mainly in the form of single metal catalysts (single-atom catalysts,[5] nanoplate catalysts,[1] nanoarray catalysts,[7] *etc.*), bimetallic catalysts,[4] metal oxides, phosphides,[6,8,9] *etc.*

Generally, wide attention has been focused on perovskite oxides with lanthanide or transition metal elements for their economic and environmental friendliness, as well as good

State Key Laboratory of Clean Energy Utilization, Zhejiang University, Hangzhou, 310027, China. E-mail: zhouhao@zju.edu.cn

† Electronic supplementary information (ESI) available. See https://doi.org/10.1039/d2se00997h

adjustability in physicochemical properties due to the tunable electronic structures and different charge distributions.[11] Yang *et al.*[12] prepared four perovskite oxide cathodes, $LaMO_{3-\delta}$ (M = Fe, Co, Ni and Cu), and innovatively applied them to electrocatalytic nitrate reduction. The Ruddlesden–Popper type La_2CuO_4 exhibited the best catalytic activity among the four perovskite oxide cathodes, with a removal rate of 11.7×10^{-3} min^{-1}. Wang *et al.*[13] successfully prepared $BiFeO_3$ flakes with a distorted perovskite-type structure and evaluated their NO_3RR electrocatalytic activities over a range of potentials. They delivered an excellent faradaic efficiency (FE) of 96.85% at −0.6 V (*vs.* the reversible hydrogen electrode, RHE) and an ammonia yield of 132.3 mg h^{-1} mg_{cat}^{-1} at −0.8 V (*vs.* RHE). In addition, only a few literature reports[14,15] have studied the effect of perovskites removing ammonia nitrogen for wastewater treatment. Among all the perovskite oxides, $LaFeO_3$ has proved to be effective in the fields of gas sensors,[16] fuel cells,[17] solid oxide electrolysis cells,[18] and the electrocatalytic hydrogen evolution reaction (HER).[19] It is worth noting that $LaFeO_3$ can even act as an electrocatalyst to reduce N_2 to NH_3 directly under ambient conditions.[20,21] However, the NH_3 yield and FE of the reaction are far from meeting the needs of industrialization.

Herein, we synthesized and applied the perovskite $LaFeO_3$ to electrochemically reduce NO_3^- to NH_3, which performed quite well as an electrocatalyst. The modified catalysts $La_xFeO_{3-\delta}$ (x = 0.95, 0.9) with A-site deficiencies were then synthesized, and plenty of oxygen vacancies were formed in the catalysts. The catalysts modified through oxygen vacancy engineering exhibited significantly increased electrocatalytic activities. The mechanism of reducing NO_3^- to NH_3 on the prepared catalysts and the reasons for the remarkable increase of electrocatalytic activities on the modified samples are proposed: the oxygen atoms in nitrate tend to fill the oxygen vacancies resulting in weakened N–O bonds. The adsorption and transformation of reaction intermediates can also be promoted due to the existence of oxygen vacancies.

2. Experimental

2.1 Chemicals

Lanthanum nitrate hexahydrate ($La(NO_3)_3 \cdot 6H_2O$, 99.9%), iron nitrate nonahydrate ($Fe(NO_3)_3 \cdot 9H_2O$, 98.5%), and citric acid monohydrate (CA, 99.5%) were purchased from Shanghai Macklin Biochemical Co., Ltd. Ethylenediamine tetraacetic acid (EDTA, AR), ammonia solution (25.0–28.0%), absolute ethanol (GR), sulphuric acid (H_2SO_4, AR), sodium sulfate (Na_2SO_4, AR), and sodium nitrate ($NaNO_3$, AR) were purchased from Sinopharm Chemical Reagent Co., Ltd. Nafion solution (5 wt%) was purchased from DuPont de Nemours, Inc. Hydrogen peroxide solution (H_2O_2, 30 wt%) was purchased from Shanghai Aladdin Biochemical Technology Co., Ltd. Ar (99.99%) was purchased from Zhejiang Otterson Gas Co., Ltd. All of the reagents were used without further purification.

2.2 Preparation of catalysts

The catalysts $La_xFeO_{3-\delta}$ (x = 1, 0.95, 0.9) were synthesized through a standard sol–gel method.[20,22] In a typical procedure, $La(NO_3)_3 \cdot 6H_2O$ and $Fe(NO_3)_3 \cdot 9H_2O$ were dissolved stoichiometrically in deionized water. EDTA and CA were then added to the metal precursor solution with the molar ratio of total metal ions: EDTA : CA = 1 : 1 : 2.5. Ammonia solution was employed to adjust the pH of the solution to ~6 so as to ensure complete complexation. A transparent gel formed after ~2 h of stirring at 90 °C. The gel was heated at 200 °C for 2.5 h in air forming a solid precursor, which was then transferred into a muffle furnace and calcined at 650 °C for 3 h in air. Finally, a reddish-brown catalyst was obtained.

2.3 Characterization

X-ray diffraction (XRD, BrukerAXS D8, Cu Kα radiation, λ = 1.54060 Å, scan rate = 5° min^{-1}) was applied to determine the composition of prepared samples and characterize the crystal structures. The microscopic morphologies and elemental composition were investigated by scanning electron microscopy (SEM, ZEISS Gemini 300, acceleration voltage = 3.0 kV) with energy dispersive spectroscopy (EDS, acceleration voltage = 15.0 kV). Inductively coupled plasma-mass spectroscopy (ICP-MS, Agilent ICPOES730) was used to determine the chemical composition of prepared catalysts. X-ray photoelectron spectroscopy (XPS, Thermo Scientific K-Alpha, Al Ka radiation, $h\nu$ = 1486.6 eV) was employed to record the composition and valence states of the elements.

2.4 Fabrication of working electrodes

First, 5 mg synthesized catalyst and 40 μL Nafion solution (5 wt%) were dispersed in 960 μL ethanol solution (V_{water} : $V_{ethanol}$ = 1 : 3) under sonication to form a homogeneous suspension. Second, 10 μL suspension was dropped and dried on the carbon paper (CP) at a time. This was repeated several times to form a covering of 1 mg cm^{-2}. Finally, the carbon paper was cut into the proper size and fixed on the platinum electrode clamp with an exposed area of 1 × 1 cm^2 to form a working electrode.

2.5 Electrochemical ammonia synthesis

The electrochemical experiments were conducted with a standard three-electrode system on an electrochemical workstation (CHI 660E, CH Instruments, Shanghai). The two cells were separated by a Nafion 117 membrane treated with 5 wt% H_2O_2 solution and 5 wt% H_2SO_4 solution at 80 °C beforehand. A Ag/AgCl electrode (saturated with KCl) and Pt foil were used as the reference electrode and the counter electrode, respectively. Before each test, Ar was bubbled through the cathode electrolyte for 30 min with magnetic stirring at the same time, followed by a cyclic voltammetry (CV) process at a scan rate of 100 mV s^{-1} to activate the catalysts and stabilize the reaction system. And bubbling and stirring were maintained during all the tests. The anode electrolyte was a 45 ml 0.1 M Na_2SO_4 solution, and the cathode electrolyte was a 45 ml 0.1 M Na_2SO_4/0.1 M $NaNO_3$ solution except for the specific control experiment where $NaNO_3$ was not added. In linear sweep voltammetry (LSV) tests, the scanning rate was set at 5 mV s^{-1}. The electrochemical reactions were tested by using amperometric i–t curves for 2 h. All

potentials throughout the paper were remarked referring to the RHE according to the Nernst equation:[10]

$$E_{RHE} = E_{Ag/AgCl} + 0.059 \times pH + 0.198$$

2.6 Determination of products

The concentration of ammonia in the cathode electrolyte after the reaction was determined by the indophenol blue method (see the ESI† for details).[11,23] The concentration of nitrite (NO_2^-) in the products was determined by a method (see the ESI† for details) reported in previous studies.[4,10] And ion chromatography (IC, Thermo Fisher Aquion) was employed to measure the concentration of NO_3^- in the electrolyte after the reaction.

The yield of NH_3 could be expressed as:

$$Y_{NH_3} = \frac{c_{NH_3} \times V}{t \times A}$$

where c_{NH_3} is the measured concentration of NH_3 (μg mL^{-1}); V is the volume of the cathode electrolyte (45 mL); t is the reaction time (2 h); A is the geometric area of the working electrode (1 cm^2).

The faradaic efficiency for NH_3 production was calculated according to the following formula:

$$FE_{NH_3} = \frac{8F \times c_{NH_3} \times V \times 10^{-6}}{M_{NH_3} \times Q}$$

where F is the Faraday constant (96485 C mol^{-1}); M_{NH_3} is the molar mass of NH_3 (17 g mol^{-1}); Q is the total charge passing through the electrode (C).

The selectivity η_x (X refers to NH_3 or NO_2^-) among all the products was defined as:

$$\eta_X = \frac{c_X / M_X}{10^3 \times c_0 - c_{NO_3^-} / M_{NO_3^-}}$$

where c_X is the measured concentration of X (μg mL^{-1}); M_X is the molar mass of X (g mol^{-1}); c_0 is the initial concentration of NO_3^- (0.1 M); $c_{NO_3^-}$ is the measured concentration of NO_3^- after the reaction (μg mL^{-1}); $M_{NO_3^-}$ is the molar mass of NO_3^- (62 g mol^{-1}).

3. Results and discussion

3.1 Characterization of the as-prepared catalysts

Fig. 1(a) shows the XRD patterns of $La_xFeO_{3-\delta}$ ($x = 1$, 0.95, 0.9, denoted as LF, $L_{0.95}F$, and $L_{0.9}F$, respectively). All three samples presented a pure orthorhombic crystal structure sharing a space group of *Pnma* (PDF#88-0641), which was consistent with previous studies.[20,22] The partially enlarged XRD patterns of the samples are displayed in Fig. 1(b). It is obvious that the main peak of the (121) plane shifted to larger angles as the value of x decreased from 1 to 0.9. This indicated the formation of A-site deficiencies in the crystal structures of $La_xFeO_{3-\delta}$ (x = 0.95, 0.9). And the lattice shrank as the concentration of A-site deficiency increased, which could be due to the tilt of the FeO_6 octahedra to fill the extra space caused by La-deficiency.[20]

The microscopic morphologies of the prepared catalysts were observed by SEM, as shown in Fig. 2(a)–(c). According to the images, it could be estimated that the particle sizes of the catalysts were about 50 nm, which was close to the results of the literature.[18] Fig. 2(d)–(f) display the EDS mapping images. It is suggested that La, Fe and O elements were distributed evenly in the prepared catalysts. And the detailed EDS spectra of LF and $L_{0.9}F$ are presented in Fig. 2(g) and (h). Besides, Table 1 shows the atomic percentage of the as-prepared catalysts measured by EDS tests. The molecular formulas of LF, $L_{0.95}F$ and $L_{0.9}F$ could be calculated accordingly to be $LaFeO_{2.54}$, $La_{0.93}FeO_{2.36}$, $La_{0.92}FeO_{2.32}$, respectively. This was consistent with the results of ICP-MS tests as shown in Table 2. The chemical compositions of LF, $L_{0.95}F$ and $L_{0.9}F$ were $La_{0.990}FeO_{3-\delta}$, $La_{0.938}FeO_{3-\delta}$, and $La_{0.915}FeO_{3-\delta}$, respectively. The above characterization results illustrate that the original $LaFeO_3$ catalyst and $La_xFeO_{3-\delta}$ (x = 0.95, 0.9) catalysts with different concentrations of A-site deficiency were successfully synthesized, which confirmed the results of XRD tests.

XPS tests were conducted in order to better confirm the elemental composition and chemical valence states of the prepared catalysts, as shown in Fig. 3. The peaks of La 3d, La 4p, La 4d, Fe 2p and O 1s could be located easily in the XPS survey spectrum (Fig. 3(a)) with the C 1s peak corresponding to the surface carbon pollution used to correct the peak position, which was consistent with the results of EDS tests. The La 3d

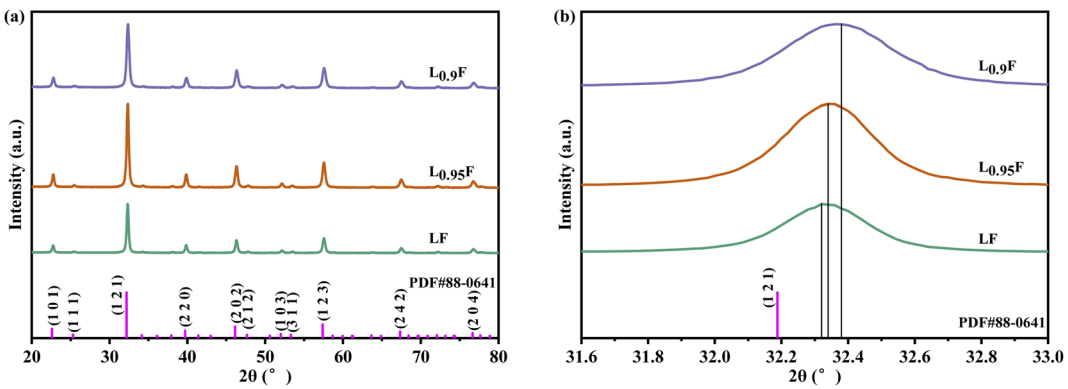

Fig. 1 (a) Overall and (b) partial XRD patterns of the as-prepared $La_xFeO_{3-\delta}$ (x = 1, 0.95, 0.9).

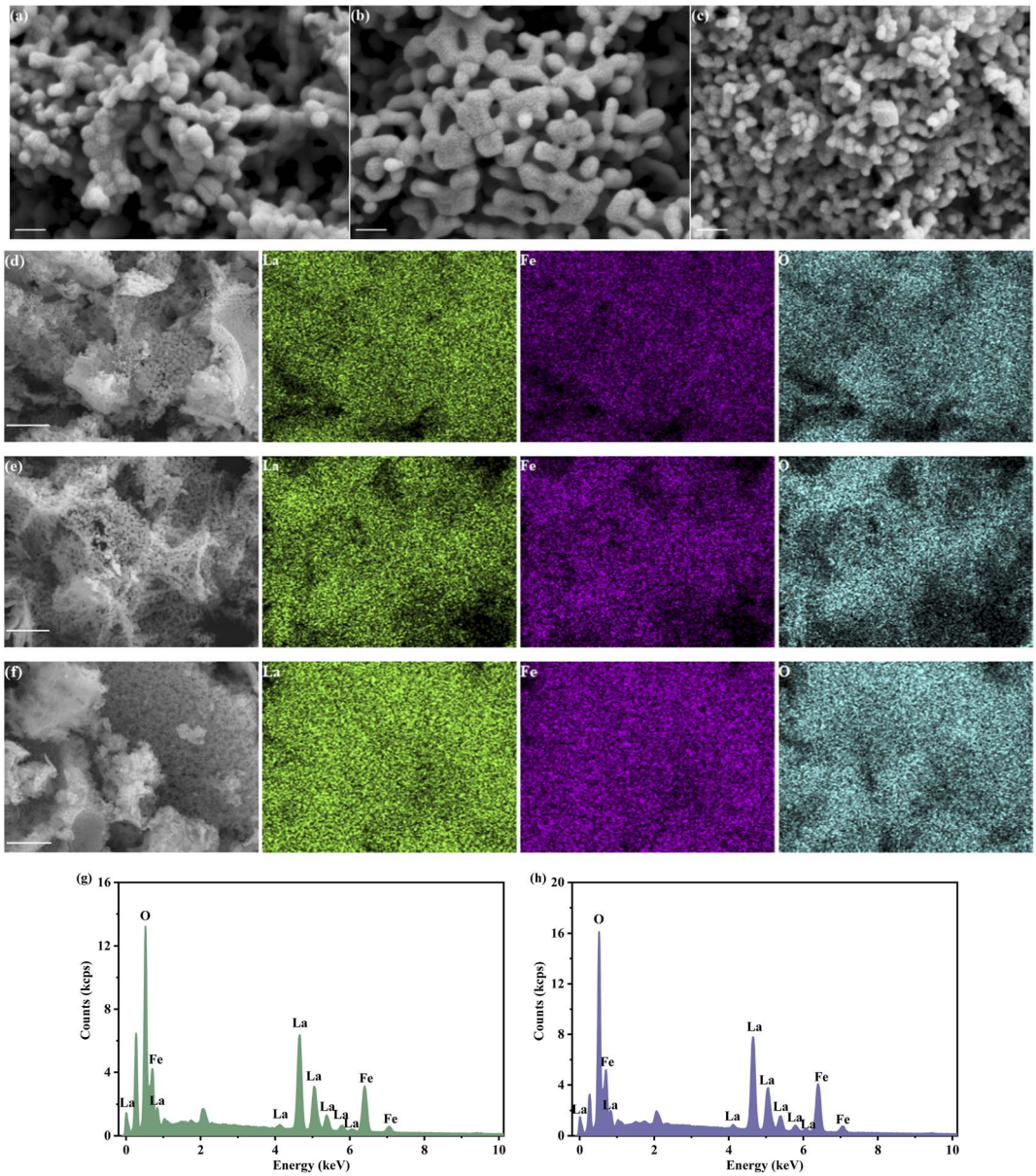

Fig. 2 SEM images of (a) LF, (b) $L_{0.95}F$, and (c) $L_{0.9}F$ (scale bar: 100 nm); EDS mappings of (d) LF, (e) $L_{0.95}F$, and (f) $L_{0.9}F$ (scale bar: 1 μm); and EDS spectra of (g) LF and (h) $L_{0.9}F$.

Table 1 Atomic percentage of the as-prepared catalysts measured from the EDS mappings

Catalyst	La (%)	Fe (%)	O (%)
LF	22.04	22.05	55.91
$L_{0.95}F$	21.74	23.31	54.95
$L_{0.9}F$	21.61	23.60	54.79

region had well-separated spin–orbit components, and each spin–orbit component was further split by multiplet splitting, as is shown in Fig. 3(b). The spin–orbit gap difference between La $3d_{5/2}$ and La $3d_{3/2}$ was calculated to be about 16.6 eV, indicating that La was at the 3+ oxidation state.[21] As shown in Fig. 3(c), the Fe 2p spectra had significantly split spin–orbit components. The peaks located at 709.6 and 710.8 eV corresponded to Fe^{2+} $2p_{3/2}$ and Fe^{3+} $2p_{3/2}$. The spin–orbit gap

Table 2 Chemical composition of the as-prepared catalysts measured by ICP-MS

	Weight percentage (%)		
Catalyst	La	Fe	ICP-MS composition
LF	56.26	22.88	$La_{0.990}FeO_{3-\delta}$
$L_{0.95}F$	52.13	22.39	$La_{0.938}FeO_{3-\delta}$
$L_{0.9}F$	53.79	23.66	$La_{0.915}FeO_{3-\delta}$

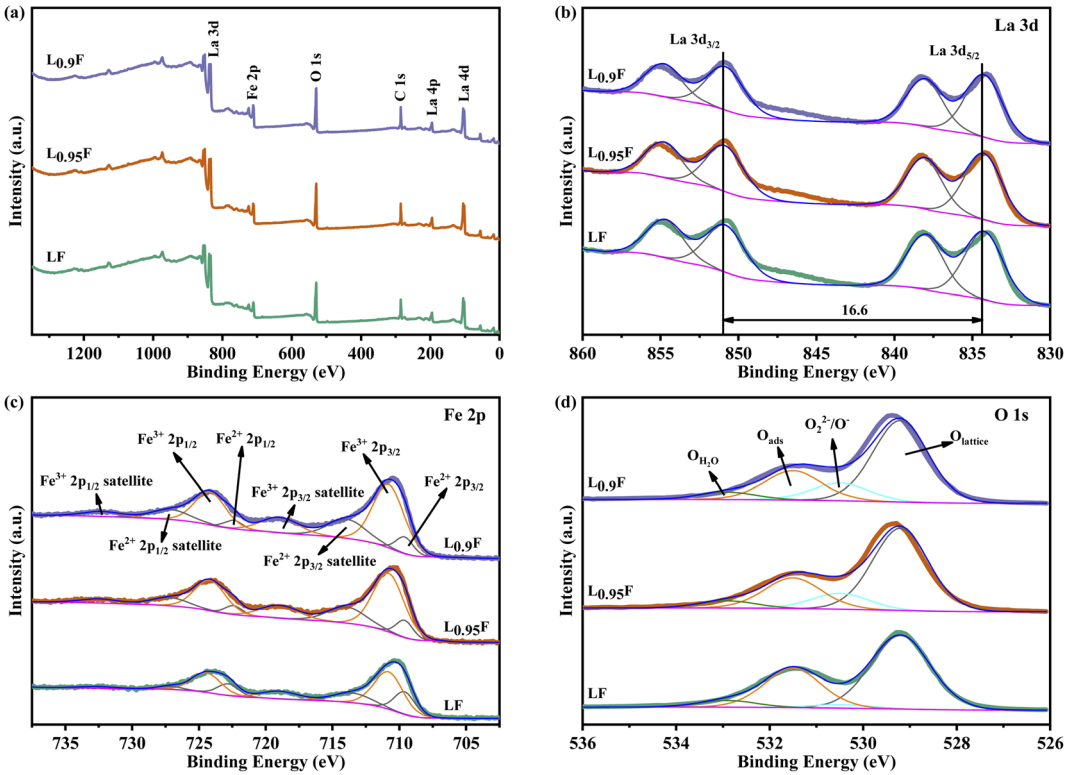

Fig. 3 (a) XPS survey, (b) La 3d, (c) Fe 2p and (d) O 1s XPS spectra of the as-prepared $La_xFeO_{3-\delta}$ ($x = 1$, 0.95, 0.9).

difference between Fe $2p_{3/2}$ and Fe $2p_{1/2}$ for both the 2+ and the 3+ oxidation states was about 13.1 eV. The satellite peaks of Fe^{2+} $2p_{3/2}$, Fe^{3+} $2p_{3/2}$, Fe^{2+} $2p_{1/2}$ and Fe^{3+} $2p_{1/2}$ could be easily identified, which further confirmed the chemical valence states of Fe^{2+} and Fe^{3+}. It is obvious in the figure that the peak area of Fe^{2+} decreased while that of Fe^{3+} increased with the increasing concentration of A-site deficiency. This illustrated the content of Fe^{2+} decreasing and that of Fe^{3+} increasing. The atomic percentage of different valence states of Fe was calculated according to the area of each peak, as is shown in Table 3. The sum of the atomic percentage of Fe^{2+} $2p_{3/2}$, Fe^{2+} $2p_{1/2}$ and Fe^{2+} satellites was 33.79% for the original LF catalyst, and it decreased to 22.44% and 22.37% for $L_{0.95}F$ and $L_{0.9}F$, respectively. In contrast, the sum of the atomic percentage of all the Fe^{3+} peaks was 66.22% for LF and increased to 77.55% and 77.62% for $L_{0.95}F$ and $L_{0.9}F$, respectively. These values confirmed the results shown in Fig. 3(c).

Fig. 3(d) shows the O 1s XPS spectra of the as-prepared $La_xFeO_{3-\delta}$ ($x = 1$, 0.95, 0.9). The peaks located at 529.2, 530.5, 531.5 and 532.9 eV corresponded to the lattice oxygen ($O_{lattice}$), highly oxidative oxygen species (O_2^{2-}/O^-), surface adsorbed oxygen or hydroxyl groups (O_{ads}), and surface-adsorbed water (O_{H_2O}), respectively.[20,22,24] And O_2^{2-}/O^- formed on the surface of prepared catalysts were closely related to the surface oxygen vacancies according to previous studies.[20,22] It can be easily concluded from the picture that the content of O_2^{2-}/O^- greatly increased after the introduction of A-site deficiency, indicating that a large number of oxygen vacancies were generated on the surface of $L_{0.95}F$ and $L_{0.9}F$ catalysts. The atomic percentage of different kinds of oxygen species estimated from the relative area of these fitted peaks is listed in Table 4. The atomic percentage of O_2^{2-}/O^- increased significantly from 2.85% for the original LF catalyst to 11.83% and 13.19% for $L_{0.95}F$ and $L_{0.9}F$, respectively, which confirms the above conclusion. Therefore, $L_{0.95}F$ and $L_{0.9}F$ catalysts were expected to exhibit outstanding electrocatalytic abilities due to the formation of a large number of oxygen vacancies.

3.2 Electrochemical experiments

LSV tests were conducted in order to estimate whether the prepared catalysts had the ability to electrochemically reduce

Table 3 Atomic percentage of different chemical valence states of Fe measured by XPS

Catalyst	Fe^{2+} $2p_{3/2}$	Fe^{2+} $2p_{3/2}$ satellite	Fe^{2+} $2p_{1/2}$	Fe^{2+} $2p_{1/2}$ satellite	Fe^{3+} $2p_{3/2}$	Fe^{3+} $2p_{3/2}$ satellite	Fe^{3+} $2p_{1/2}$	Fe^{3+} $2p_{1/2}$ satellite
LF	11.83	6.43	14.13	1.4	27.33	5.1	32.67	1.12
$L_{0.95}F$	5.13	7.46	6.13	3.72	31.71	5.96	37.89	1.99
$L_{0.9}F$	4.6	8.03	5.49	4.25	31.41	6.49	37.54	2.18

Table 4 Atomic percentage of different kinds of oxygen species measured by XPS

Catalyst	$O_{lattice}$	O_2^{2-}/O^-	O_{ads}	O_{H_2O}
LF	60.73	2.85	31.11	5.32
$L_{0.95}F$	59.75	11.83	23.02	5.40
$L_{0.9}F$	59.20	13.19	22.08	5.53

nitrate. Fig. 4(a) shows the LSV curves of $La_xFeO_{3-\delta}$ ($x = 1$, 0.95, 0.9) loaded and bare carbon paper in the electrolyte with and without NO_3^-. The results illustrate that the current density flowing through the electrodes loaded with any catalyst was larger than that of bare carbon paper whether in the electrolyte with or without nitrate. This confirmed the good electrocatalytic performance of the prepared catalysts. For any of the prepared catalysts, the current density in the electrolyte containing nitrate was significantly larger than that without nitrate in the potential range of −0.4 to −1.0 V (*vs.* RHE). This was powerful evidence that the prepared catalysts could electrocatalytically reduce nitrate in the potential range. Moreover, the current density for $L_{0.95}F$ and $L_{0.9}F$ was significantly larger than that for LF in the electrolyte containing nitrate, which illustrated that $La_xFeO_{3-\delta}$ with A-site deficiencies was expected to show stronger abilities of reducing nitrate. This could be attributed to the promotion of nitrate reduction by the presence of oxygen vacancies, which was consistent with previous reports.[3,25–29] It was worth noting that the current density of $L_{0.9}F$ in the electrolyte without nitrate was remarkably lower than that of LF. This proved that the oxygen vacancies could even suppress the competitive HER.[26]

The experimental results of electrocatalytically reducing nitrate on $La_xFeO_{3-\delta}$ ($x = 1$, 0.95, 0.9) catalysts at −0.7 V are presented in Fig. 4(b) (see Fig. S3 in the ESI† for the chronoamperometry curves). The original LF catalyst exhibited the ability to synthesize NH_3 with a yield of 49.0 μg h^{-1} cm^{-2}. The NH_3 yield was significantly increased after the introduction of oxygen vacancies. $L_{0.95}F$ and $L_{0.9}F$ exhibited NH_3 yields of 128.1 and 140.9 μg h^{-1} cm^{-2}, respectively, which were 2.6 times and 2.9 times the value for the original LF catalyst. The faradaic efficiency was substantially increased from 50.7% for LF to 65.6% and 61.7% for $L_{0.95}F$ and $L_{0.9}F$, respectively. This also proved that the introduction of oxygen vacancies obviously had a positive effect on the activities of the electrocatalysts, which could be attributed to two reasons. For one thing, the oxygen atoms in the nitrate tended to fill the oxygen vacancies resulting in the weakened N–O bonds.[25] For another, the oxygen vacancies optimized the charge distribution and served as the active sites of the catalysts, bringing about improved charge transfer efficiency and the promoted adsorption and transformation of reaction intermediates.[3,30,31]

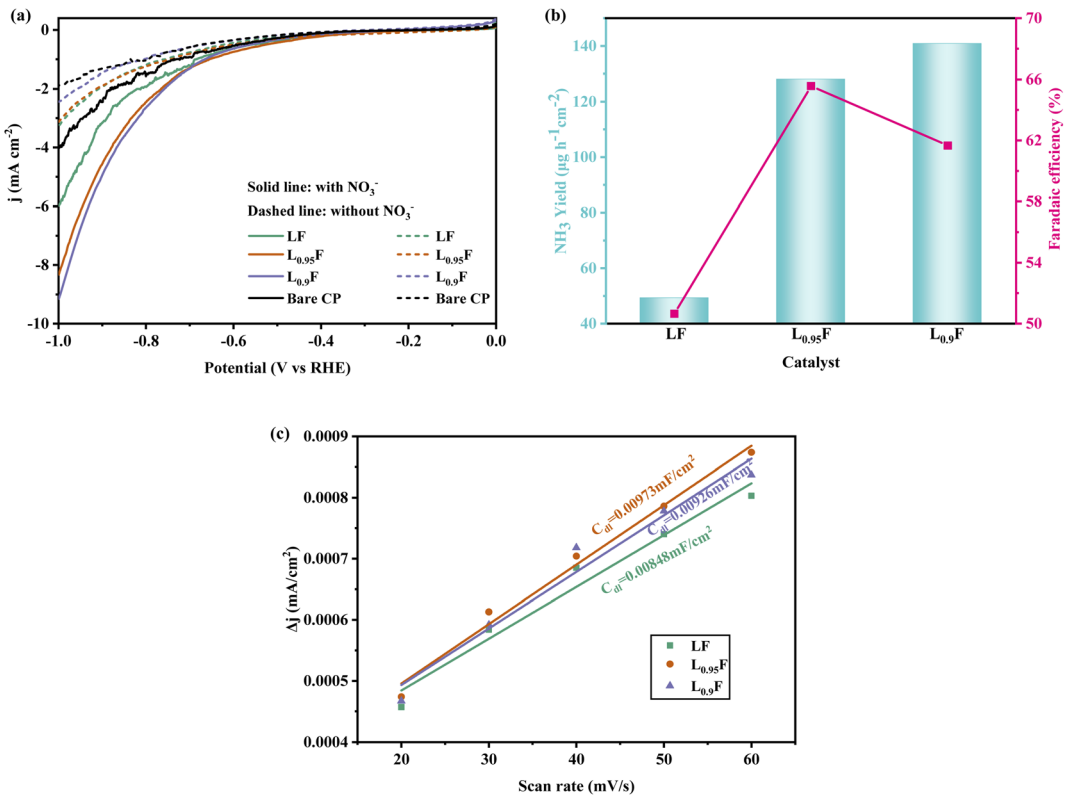

Fig. 4 (a) LSV curves of $La_xFeO_{3-\delta}$ ($x = 1$, 0.95, 0.9) loaded and bare carbon paper in the electrolyte with and without NO_3^-; (b) NH_3 yields and faradaic efficiencies of electrocatalytic reduction of nitrate on $La_xFeO_{3-\delta}$ ($x = 1$, 0.95, 0.9) catalysts at −0.7 V (*vs.* RHE); (c) current density differences plotted *versus* scan rates on $La_xFeO_{3-\delta}$ ($x = 1$, 0.95, 0.9) electrodes.

The catalytic activities of materials can be evaluated from the electrochemically active surface area (ECSA), which is positively correlated with the double layer capacitance (C_{dl}) of the electrochemical system. A series of cyclic voltammetry (CV) tests were conducted on electrodes loaded with different catalysts in the non-faradaic region to estimate the C_{dl} (see Fig. S5–S7 in the ESI† for the CV curves). The current density differences on $La_xFeO_{3-\delta}$ ($x = 1$, 0.95, 0.9) electrodes were plotted *versus* scan rates derived from the CV curves, as shown in Fig. 4(c). The slopes obtained by linear fitting are the C_{dl} of the electrochemical system. When the $L_{0.95}F$ and $L_{0.9}F$ electrodes were employed, the C_{dl} was 0.00973 and 0.00926 mF cm^{-2}, respectively, which was better than that when the LF electrode was used (0.00848 mF cm^{-2}). Therefore, the ECSA of different catalysts was in the order of $L_{0.95}F$ > $L_{0.9}F$ > LF. This was consistent with the order of faradaic efficiency of different catalysts, indicating that oxygen vacancies could promote the electrochemical activities of the catalysts.

Experiments of nitrate reduced electrocatalytically on the $L_{0.9}F$ catalyst at different potentials were carried out, as Fig. 5(a) shows (see Fig. S4 in the ESI† for the chronoamperometry curves). As the potential moved to a more negative direction, the yield of ammonia increased significantly from 140.9 μg h^{-1} cm^{-2} at −0.7 V to 1024.8 μg h^{-1} cm^{-2} at −1.0 V, and the latter was even 7.3 times the former. Meanwhile, the faradaic efficiency of NO_3^--to-NH_3 first increased from 61.7% at −0.7 V to 78.1% at −0.8 V, reaching the maximum value. Then the faradaic efficiency decreased to 66.5% at −0.9 V and increased slightly to 70.2% at −1.0 V. The decrease of the faradaic efficiency could be attributed to the competitive HER process in the potential range from −0.8 V to more negative.[1] Table 5 compares the catalytic performance of $L_{0.9}F$ with other related catalysts. $L_{0.9}F$ showed the prominent faradaic efficiency among iron-based catalysts,[5,6] perovskite catalysts[12,13] or oxygen vacancy-rich catalysts.[25–27]

In addition to NH_3, the electrocatalytic reduction reaction of nitrate also produced a small amount of the byproduct, NO_2^-. Fig. 5(b) shows the selectivity of NO_3^--to-NH_3 and NO_3^--to-NO_2^- on the $L_{0.9}F$ catalyst at different potentials. As the potential became more negative, the selectivity for NH_3 in the products increased remarkably from 1.1% at −0.7 V to 7.5% at −1.0 V, which was nearly 7 times the former. This explained the slight recovery of the faradaic efficiency when the potential varied from −0.9 to −1.0 V. As for the byproduct, NO_2^-, the selectivity increased slightly but remained at a low level (less than 2%) consistently when the potential varied from −0.7 to −1.0 V.

Fig. 5(c) shows the experimental results of consecutive recycling tests on $L_{0.9}F$ at −0.8 V. The NH_3 yield maintained at a high level after several cycles and was up to 572.5 μg h^{-1} cm^{-2} for the fourth cycle and was even slightly higher than that for the first cycle (463.4 μg h^{-1} cm^{-2}). The faradaic efficiency decreased slightly after recycling but was still as high as 73.6% for the fourth cycle. The consecutive recycling tests proved that

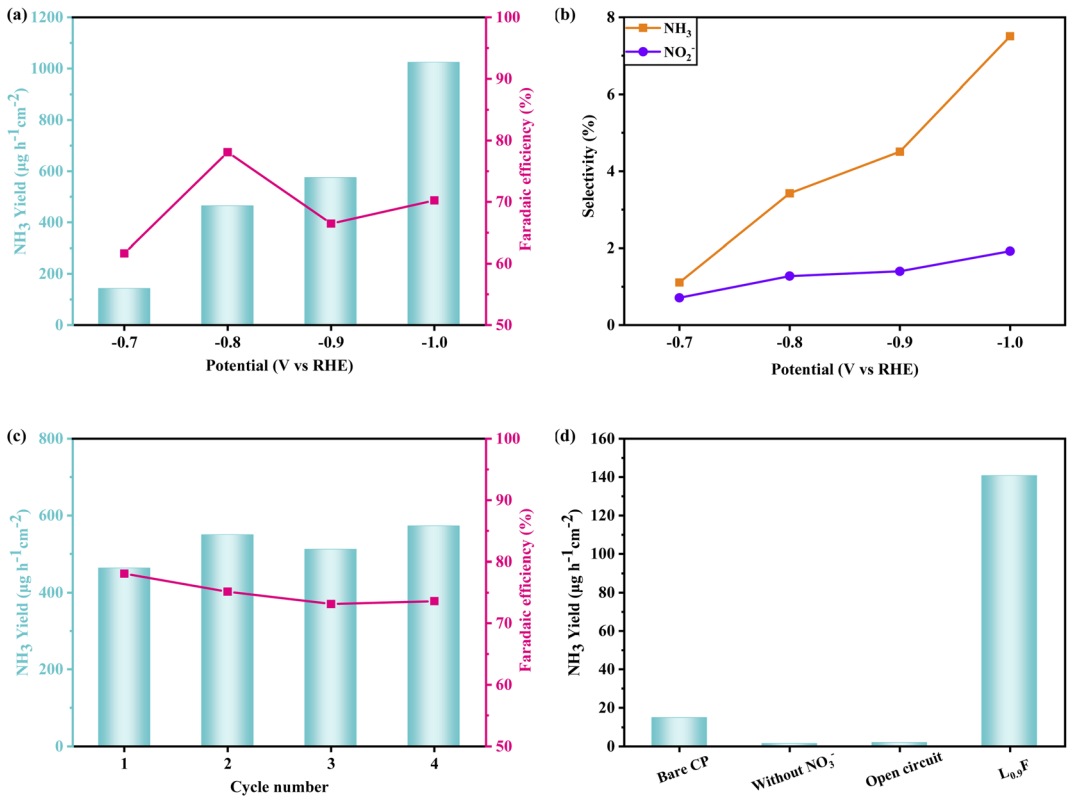

Fig. 5 (a) NH_3 yields and faradaic efficiencies and (b) NH_3 and NO_2^- selectivities among products of electrocatalytic reduction of nitrate on $L_{0.9}F$ at different potentials; (c) consecutive recycling tests on $L_{0.9}F$ at −0.8 V (*vs.* RHE); (d) control experiments under different conditions.

Table 5 Comparison of catalytic performance of $L_{0.9}F$ with other related catalysts

Catalyst	Reaction condition	NH_3 yield	Faradaic efficiency	Ref.
Fe single atom	0.1 M K_2SO_4/0.5 M KNO_3	0.46 mmol h^{-1} cm^{-2} at −0.85 V (*vs.* RHE)	~75% at −0.66 V (*vs.* RHE)	5
Co-doped Fe/Fe_2O_3	0.1 M Na_2SO_4/500 ppm $NaNO_3$	1505.9 μg h^{-1} cm^{-2} at −0.95 V (*vs.* RHE)	85.2% at −0.75 V (*vs.* RHE)	6
La_2CuO_4	0.05 M Na_2SO_4/50 mg L^{-1} $NaNO_3$	—	29.3% at −1.0 V (*vs.* SCE)	12
$BiFeO_3$	0.1 M KOH/0.1 M KNO_3	132.3 mg h^{-1} mg_{cat}^{-1} at −0.8 V (*vs.* RHE)	96.85% at −0.6 V (*vs.* RHE)	13
TiO_{2-x}	0.5 M Na_2SO_4/50 ppm NO_3^--N	0.045 mmol h^{-1} mg_{cat}^{-1} at −1.6 V (*vs.* SCE)	85.0% at −1.6 V (*vs.* SCE)	25
Nb_2O_{5-x}	0.5 M Na_2SO_4/50 ppm NO_3^--N	0.287 mmol h^{-1} cm^{-2} at −1.1 V (*vs.* RHE)	85.1% at −1.1 V (*vs.* RHE)	26
Cu/TiO_{2-x}	0.5 M Na_2SO_4/200 ppm NO_3^--N	0.1143 mmol h^{-1} mg_{cat}^{-1} at −0.75 V (*vs.* RHE)	81.34% at −0.75 V (*vs.* RHE)	27
$L_{0.9}F$ (namely $La_{0.9}FeO_{3-\delta}$)	0.1 M Na_2SO_4/0.1 M $NaNO_3$	1024.8 μg h^{-1} cm^{-2} at −1.0 V (*vs.* RHE)	78.1% at −0.8 V (*vs.* RHE)	This work

the prepared catalysts had excellent stability and were expected to be put into cyclic utilization in the industry in the future.

Control experiments under different conditions were conducted in order to prove that the NH_3 produced in this paper was formed by the electrochemical reduction of NO_3^- on the prepared catalysts, as is shown in Fig. 5(d). The results illustrate that the NH_3 yield was only 14.5 μg h^{-1} cm^{-2} with the bare carbon paper as the working electrode at −0.7 V, which was negligible compared with the value for the electrode loaded with $L_{0.9}F$ (140.9 μg h^{-1} cm^{-2}) under the same circumstances. In addition, almost no NH_3 was detected in the electrolyte when NO_3^- was not added to the electrolyte or the potential was set to the open-circuit voltage. Therefore, the NH_3 produced in this paper was confirmed to be formed from the electrocatalytic reduction of NO_3^- on the prepared catalysts.

Fig. 6 shows the schematic model of the electrocatalytic NO_3^--to-NH_3 process on the modified catalysts $La_xFeO_{3-\delta}$ (x = 0.95, 0.9) with A-site deficiency. It is well known that the electrochemical NO_3RR process can be divided into two stages.[28] In stage I, NO_3^- is adsorbed and converted to NO_2*, which is the rate-determining step. In stage II, NO_2* is converted to products, which is the selectivity-determining step. When A-site deficiencies are formed due to the lack of La in the catalysts, oxygen vacancies are generated on the surface of the catalysts in order to achieve the charge balance. The oxygen atoms in NO_3^- tend to fill the oxygen vacancies to form NO_3*, resulting in the lower adsorption energy of NO_3^- on $La_xFeO_{3-\delta}$ (x = 0.95, 0.9) than on the original $LaFeO_3$ catalyst.[27–29] And the N–O bonds in NO_3* are broken to form NO_2* by adsorbing protons coupled with electrons.[25] Similarly, the oxygen atoms in NO_2* are easy to capture by oxygen vacancies, and the N–O bonds are broken to form NO*.[28,29] Another explanation is that NO_2* experiences a more favorable hydrogenation (hydrogenation on oxygen) to form NO* on oxygen vacancy-rich catalysts instead of hydrogenation on nitrogen occurring on catalysts without oxygen vacancies, which effectively inhibits the formation of by-products (NO_2 and HNO_2).[27] Subsequently, NO* is gradually converted to HNO*, NH*, NH_2*, and finally NH_3* after a series of hydrogenation reactions.[29] Therefore, $La_xFeO_{3-\delta}$ (x = 0.95, 0.9) can afford outstanding NH_3 yield, faradaic efficiency and selectivity due to the promoted adsorption and conversion of NO_3^- in stage I and the enhanced NO_2*-NH_3 process in stage II. Besides, previous studies have illustrated that oxygen vacancies can serve as the active sites of the catalysts to facilitate reactions at low overpotentials; deficiencies on the surface of catalysts can optimize the charge distribution and the conductivity of catalysts, and the charge transfer efficiency between the catalysts and electrolytes is effectively enhanced.[3,30,31]

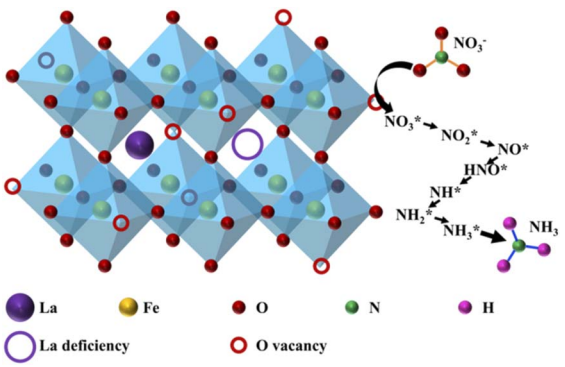

Fig. 6 Schematic model of the electrocatalytic NO_3^--to-NH_3 process on the modified catalysts $La_xFeO_{3-\delta}$ (x = 0.95, 0.9) with A-site deficiency.

4. Conclusions

In summary, we synthesized perovskite $LaFeO_3$ through a standard sol–gel method and innovatively applied it to the electrocatalytic reduction of nitrate to ammonia, which performed quite well as an electrocatalyst. And then the A-site deficiency was successfully introduced into the lattice of the original $LaFeO_3$ so that plenty of oxygen vacancies were confirmed to be generated in the modified catalysts $La_xFeO_{3-\delta}$ (x = 0.95, 0.9). The activities of the catalysts were greatly improved after being

modified through oxygen vacancy engineering. $L_{0.95}F$ and $L_{0.9}F$ exhibited NH_3 yields of 128.1 and 140.9 μg h^{-1} cm^{-2}, respectively, after 2 hours of the electrochemical process at −0.7 V (*vs.* RHE), which were 2.6 times and 2.9 times the value for the original LF catalyst (49.0 μg h^{-1} cm^{-2}). The faradaic efficiency was substantially increased from 50.7% for LF to 65.6% and 61.7% for $L_{0.95}F$ and $L_{0.9}F$, respectively. For the catalyst $L_{0.9}F$, the highest NH_3 yield was up to 1024.8 μg h^{-1} cm^{-2} at −1.0 V (*vs.* RHE), while the maximum faradaic efficiency was 78.1% achieved at −0.8 V (*vs.* RHE). The consecutive recycling experiments proved the excellent stability of the prepared catalysts, and the NH_3 produced in this paper was confirmed to be formed from the electrocatalytic reduction of NO_3^- on the prepared catalysts. According to the above work and results, a schematic model of the electrocatalytic NO_3^--to-NH_3 process on the modified catalysts $La_xFeO_{3-\delta}$ (x = 0.95, 0.9) with A-site deficiency was proposed: the oxygen atoms in nitrate tend to fill the oxygen vacancies resulting in the weakened N–O bonds. The adsorption and transformation of reaction intermediates can also be promoted due to the existence of oxygen vacancies. Besides, the oxygen vacancies can serve as the active sites of the catalysts, and the deficiencies can optimize the charge distribution and enhance the charge transfer efficiency. These conclusions provide new inspiration for the selection and improvement of electrocatalysts for synthesizing ammonia from the reduction of nitrate.

Author contributions

Qi Yin: conceptualization, methodology, validation, formal analysis, investigation, data curation, writing – original draft, and writing – review & editing. Shihao Hu: investigation, data curation, and writing – review & editing. Jingwen Liu: investigation. Hao Zhou: conceptualization, resources, writing – review & editing, supervision, project administration, and funding acquisition.

Conflicts of interest

There are no conflicts to declare.

Acknowledgements

This research did not receive any specific grant from funding agencies in the public, commercial, or not-for-profit sectors.

References

1 Y. Xu, M. Wang, K. Ren, T. Ren, M. Liu, Z. Wang, X. Li, L. Wang and H. Wang, Atomic defects in pothole-rich two-dimensional copper nanoplates triggering enhanced electrocatalytic selective nitrate-to-ammonia transformation, *J. Mater. Chem. A*, 2021, **9**(30), 16411–16417.

2 G. Chen, Y. Yuan, H. Jiang, S. Ren, L. Ding, L. Ma, T. Wu, J. Lu and H. Wang, Electrochemical reduction of nitrate to ammonia via direct eight-electron transfer using a copper–molecular solid catalyst, *Nat. Energy*, 2020, **5**(8), 605–613.

3 H. Wang, Q. Mao, T. Ren, T. Zhou, K. Deng, Z. Wang, X. Li, Y. Xu and L. Wang, Synergism of Interfaces and Defects: Cu/Oxygen Vacancy-Rich Cu-Mn_3O_4 Heterostructured Ultrathin Nanosheet Arrays for Selective Nitrate Electroreduction to Ammonia, *ACS Appl. Mater. Interfaces*, 2021, **13**(37), 44733–44741.

4 C. Wang, Z. Liu, T. Hu, J. Li, L. Dong, F. Du, C. Li and C. Guo, Metasequoia-like Nanocrystal of Iron-Doped Copper for Efficient Electrocatalytic Nitrate Reduction into Ammonia in Neutral Media, *ChemSusChem*, 2021, **14**(8), 1825–1829.

5 Z. Wu, M. Karamad, X. Yong, Q. Huang, D. A. Cullen, P. Zhu, C. Xia, Q. Xiao, M. Shakouri, F. Chen, J. Y. Kim, Y. Xia, K. Heck, Y. Hu, M. S. Wong, Q. Li, I. Gates, S. Siahrostami and H. Wang, Electrochemical ammonia synthesis via nitrate reduction on Fe single atom catalyst, *Nat. Commun.*, 2021, **12**, 2870.

6 S. Zhang, M. Li, J. Li, Q. Song and X. Liu, High-ammonia selective metal–organic framework–derived Co-doped Fe/Fe_2O_3 catalysts for electrochemical nitrate reduction, *Proc. Natl. Acad. Sci. U. S. A.*, 2022, **119**(6), e2115504119.

7 X. Deng, Y. Yang, L. Wang, X. Z. Fu and J. L. Luo, Metallic Co Nanoarray Catalyzes Selective NH_3 Production from Electrochemical Nitrate Reduction at Current Densities Exceeding 2 A cm^{-2}, *Adv. Sci.*, 2021, **8**(7), 2004523.

8 Q. Hong, J. Zhou, Q. Zhai, Y. Jiang, M. Hu, X. Xiao, S. Li and Y. Chen, Cobalt phosphide nanorings towards efficient electrocatalytic nitrate reduction to ammonia, *Chem. Commun.*, 2021, **57**(88), 11621–11624.

9 Q. Yao, J. Chen, S. Xiao, Y. Zhang and X. Zhou, Selective Electrocatalytic Reduction of Nitrate to Ammonia with Nickel Phosphide, *ACS Appl. Mater. Interfaces*, 2021, **13**(26), 30458–30467.

10 P. Gao, Z. H. Xue, S. N. Zhang, D. Xu, G. Y. Zhai, Q. Y. Li, J. S. Chen and X. H. Li, Schottky Barrier-Induced Surface Electric Field Boosts Universal Reduction of NO_x^- in Water to Ammonia, *Angew. Chem., Int. Ed.*, 2021, **60**(38), 20711–20716.

11 X. Hu, Y. Sun, S. Guo, J. Sun, Y. Fu, S. Chen, S. Zhang and J. Zhu, Identifying electrocatalytic activity and mechanism of $Ce_{1/3}NbO_3$ perovskite for nitrogen reduction to ammonia at ambient conditions, *Appl. Catal., B*, 2021, **280**, 119419.

12 W. Yang, L. Yang, H. Peng, S. Lv, H. Muhammad Adeel Sharif, W. Sun, W. Li, C. Yang and H. Lin, Perovskite oxide $LaMO_{3-\delta}$ (M = Fe, Co, Ni and Cu) cathode for efficient electroreduction of nitrate, *Sep. Purif. Technol.*, 2022, **295**, 121278.

13 J. Wang, D. Wu, M. Li, X. Wei, X. Yang, M. Shao and M. Gu, Bismuth Ferrite as an Electrocatalyst for the Electrochemical Nitrate Reduction, *Nano Lett.*, 2022, **22**, 5600–5606.

14 Y. Zhang, Z. Jin, L. Chen and J. Wang, $SrFe_xNi_{1-x}O_{3-\delta}$ Perovskites Coated on Ti Anodes and Their Electrocatalytic Properties for Cleaning Nitrogenous Wastewater, *Materials*, 2019, **12**(3), 511.

15 L. Chen, Y. Zhang and C. Ma, Perovskites $Sr_xLa_{1-x}Mn_yCo_{1-y}O_{3-\delta}$ coated on Ti as stable non-noble anode for efficient electrocatalytic oxidation of organic

wastewater containing ammonia nitrogen, *Chem. Eng. J.*, 2020, **393**, 124514.

16 A. Queraltó, D. Graf, R. Frohnhoven, T. Fischer, H. Vanrompay, S. Bals, A. Bartasyte and S. Mathur, $LaFeO_3$ Nanofibers for High Detection of Sulfur-Containing Gases, *ACS Sustainable Chem. Eng.*, 2019, **7**(6), 6023–6032.

17 M. Noroozifar, M. Khorasani-Motlagh, M. Ekrami-Kakhki and R. Khaleghian-Moghadam, Enhanced electrocatalytic properties of Pt–chitosan nanocomposite for direct methanol fuel cell by $LaFeO_3$ and carbon nanotube, *J. Power Sources*, 2014, **248**, 130–139.

18 S. Hu, L. Zhang, Z. Cao, W. Yu, P. Zhang, X. Zhu and W. Yang, Cathode activation process and CO_2 electroreduction mechanism on $LnFeO_{3-\delta}$ (Ln=La, Pr and Gd) perovskite cathodes, *J. Power Sources*, 2021, **485**, 229343.

19 A. Galal, H. K. Hassan, N. F. Atta and T. Jacob, An Efficient and Durable Electrocatalyst for Hydrogen Production Based on Earth-Abundant Oxide-Graphene Composite, *ChemistrySelect*, 2017, **2**(31), 10261–10270.

20 K. Chu, F. Liu, J. Zhu, H. Fu, H. Zhu, Y. Zhu, Y. Zhang, F. Lai and T. Liu, A General Strategy to Boost Electrocatalytic Nitrogen Reduction on Perovskite Oxides via the Oxygen Vacancies Derived from A-Site Deficiency, *Adv. Energy Mater.*, 2021, **11**(11), 2003799.

21 C. Li, D. Ma, S. Mou, Y. Luo, B. Ma, S. Lu, G. Cui, Q. Li, Q. Liu and X. Sun, Porous $LaFeO_3$ nanofiber with oxygen vacancies as an efficient electrocatalyst for N_2 conversion to NH_3 under ambient conditions, *J. Energy Chem.*, 2020, **50**, 402–408.

22 Y. Zhu, W. Zhou, J. Yu, Y. Chen, M. Liu and Z. Shao, Enhancing Electrocatalytic Activity of Perovskite Oxides by Tuning Cation Deficiency for Oxygen Reduction and Evolution Reactions, *Chem. Mater.*, 2016, **28**(6), 1691–1697.

23 Z. Wang, J. Shen, W. Fu, J. Liao, J. Dong, P. Zhuang, Z. Cao, Z. Ye, J. Shi and M. Ye, Controlled oxygen vacancy engineering on In_2O_{3-x}/CeO_{2-y} nanotubes for highly selective and efficient electrocatalytic nitrogen reduction, *Inorg. Chem. Front.*, 2020, **7**, 3609.

24 Y. Cong, Z. Geng, Y. Sun, L. Yuan, X. Wang, X. Zhang, L. Wang, W. Zhang, K. Huang and S. Feng, Cation Segregation of A-Site Deficiency Perovskite $La_{0.85}FeO_{3-\delta}$ Nanoparticles toward High-Performance Cathode Catalysts for Rechargeable Li-O_2 Battery, *ACS Appl. Mater. Interfaces*, 2018, **10**(30), 25465–25472.

25 R. Jia, Y. Wang, C. Wang, Y. Ling, Y. Yu and B. Zhang, Boosting Selective Nitrate Electroreduction to Ammonium by Constructing Oxygen Vacancies in TiO_2, *ACS Catal.*, 2020, **10**(6), 3533–3540.

26 B. Cao, X. Xu, Z. Hong, J. Liao, P. Li, H. Zhang and S. Duo, Oxygen-vacancy-containing Nb_2O_5 nanorods with modified semiconductor character for boosting selective nitrate-to-ammonia electroreduction, *Sustainable Energy Fuels*, 2022, **6**(8), 2062–2066.

27 X. Zhang, C. Wang, Y. Guo, B. Zhang, Y. Wang and Y. Yu, Cu clusters/TiO_{2-x} with abundant oxygen vacancies for enhanced electrocatalytic nitrate reduction to ammonia, *J. Mater. Chem. A*, 2022, **10**(12), 6448–6453.

28 Y. Wang, S. Shu, M. Peng, L. Hu, X. Lv, Y. Shen, H. Gong and G. Jiang, Dual-site electrocatalytic nitrate reduction to ammonia on oxygen vacancy-enriched and Pd-decorated MnO_2 nanosheets, *Nanoscale*, 2021, **13**(41), 17504–17511.

29 Y. Wang, H. Li, W. Zhou, X. Zhang, B. Zhang and Y. Yu, Structurally Disordered RuO_2 Nanosheets with Rich Oxygen Vacancies for Enhanced Nitrate Electroreduction to Ammonia, *Angew. Chem., Int. Ed.*, 2022, **61**, e202202604.

30 T. Sun, G. Zhang, D. Xu, X. Lian, H. Li, W. Chen and C. Su, Defect chemistry in 2D materials for electrocatalysis, *Mater. Today Energy*, 2019, **12**, 215–238.

31 Y. Jia, K. Jiang, H. Wang and X. Yao, The Role of Defect Sites in Nanomaterials for Electrocatalytic Energy Conversion, *Chem*, 2019, **5**(6), 1371–1397.